

Magnetic Field Aided Indoor Navigation

William F. Storms, Air Force Institute of Technology

John F. Raquet, Air Force Institute of Technology

Biography

Will Storms is currently a developmental engineer at the Air Force Research Laboratory. He has recently completed his Masters of Science in Electrical Engineering at the Air Force Institute of Technology.

John Raquet currently serves as an Associate Professor of Electrical Engineering at the Air Force Institute of Technology, where he is also the Director of the Advanced Navigation Technology (ANT) Center. He has been working in navigation-related research for over 18 years.

1 Introduction

The position solutions provided by global navigation satellite systems (GNSS) have provided sub-meter level accuracy in many applications, but the positioning solutions from these types of navigational aids are only available when the receiver has uninterrupted access to at least four satellites [5]. While overall satellite coverage of the Earth has increased, environments such as urban canyons and inside buildings can prevent the acquisition of the required satellite signals. Without adequate satellite coverage, the sub-meter level positioning solutions cannot be obtained. At the same time, there is an increasing desire to develop autonomous, miniature vehicles. The navigation of these systems is generally completed with inertial navigation systems aided by GNSS position solutions. If the GNSS position solutions are not available, these miniature vehicles will not be able to navigate with the required level of accuracy. This paper investigates the feasibility of using magnetic fields to aid an inertial system when GNSS signals are not available.

This paper presents the uniqueness of magnetic field variations from one location to the next in an indoor environment. Using this uniqueness, the feasibility of using magnetic field variations to accurately estimate the trajectory of a vehicle is demonstrated. Finally, the magnetic aided position algorithm developed to estimate a vehicle's trajectory is applied to a vehicle tracking implementation. The following paper examines the spatial variations of magnetic field intensities, but does not include an in-depth analysis of the variations with respect to time.

The methods proposed, and used, in the current paper implement a terrain navigation algorithm, where the terrain map is replaced by a map of magnetic field intensities, to determine the position based on the measured magnetic field intensity. The approach presented in this research is based on a multiple beam terrain navigation approach originally developed for submarine navigation [7]. However, the algorithm has been adapted to use a magnetic field intensity map instead of a terrain map and three-axis magnetometers instead of a depth/terrain height measuring device.

The magnetic aided position algorithm is demonstrated by estimating a vehicle's trajectory using a magnetic field intensity map of the entire area to be traversed. The position estimate of the on-board inertial system is combined with the position measurement from the magnetic aided position algorithm using a Kalman filter (KF).

2 Magnetic Field Based Navigation

Magnetic fields have been observed by humans for centuries. Plato wrote of rocks that were magnetically attracted to other rocks in 400 BC [1]. The Chinese developed a magnetic compass between 300 and 200 BC that was used to align construction with the Earth's magnetic fields [1]. From these early observations and uses, merchants began using compasses to navigate to their various trading locations. This was the start of the compass navigation used to today. As demonstrated by Columbus and many other early explorers, not understanding the nature of the Earth's magnetic field can cause confusion when trying to use the Earth's magnetic field to navigate on the Earth [1].

2.1 Brief Description of the Earth's Magnetic Field

The magnetic field that surrounds the Earth comes from currents that are induced by "the outer-core region of the Earth", which is composed of "a hot and dense liquid of highly conducting nickel-iron", and "the Earth's spin and shape" [1]. Together these characteristics form a current-loop that generates a magnetic field that acts similar to a dipole magnet. Figure 1 shows the different layers of the Earth, as well as the magnetic field surrounding it [1]. From this illustra-

tion, it can be seen that the Earth’s magnetic field can be observed from any position on the Earth. While the main field of the Earth’s magnetic field is fairly constant, there are a number of factors that can cause variation in the intensity of the magnetic field at any given time and place.

Campbell highlights two of the naturally occurring variations. The first is caused by an alteration in the Earth’s electrical conductivity, which can be caused by “a major change in the groundwater content at a deep subsurface fracture. . .or when a highly conductive active magma chamber at a volcanic site moves before an eruption” [1]. The second cause is a result of a change in the magnetic domain boundaries of rocks due to increased external stress [1]. Campbell describes this by stating this change is brought about “as a result of the loading of rock surfaces as a major dam is filled or at a volcano as a result of a change in the magma chamber pressure on the surrounding rock material” [1].

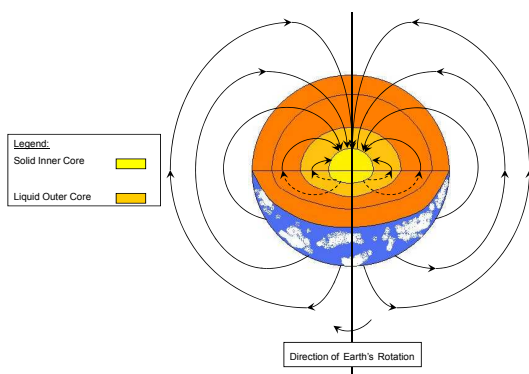


Figure 1: Illustration of the Earth’s main dipole magnetic field. The liquid outer core, along with the Earth’s rotation is believed to be the source of the Earth’s dipole like magnetic field [1].

In addition to variations of this nature, deposits in the Earth’s crust also contribute to local variations in the observed magnetic field [12, 6]. These local variations have more of an effect closer to the Earth’s surface. As altitude is increased, the intensity of the magnetic field has less variation due to these deposits in the crust [12, 6]. Some other factors that can add to these variations are the effects on the Earth’s magnetic field due to magnetic storms, the moon, the sun, and the ionosphere [6].

There are also artificial disturbances that perturb the Earth’s magnetic field [6]. These artificial disturbances are caused by electrical currents running through any type of metal or conducting structure. In buildings, walls are often reinforced with steel rebar

and new construction projects use steel studs in interior walls. Steel beams used to support the floors of buildings add to the problem, as well as pipes, wires, and electric motors or equipment [6, 8]. These artificial disturbances are the signals of primary interest in this paper.

2.2 Use of Magnetic Fields in Navigation Today

In robotics applications, magnetic fields are used to determine which direction a vehicle is facing, also known as its heading [8]. This is an important tool as vehicles become smaller because heading measurements generally come from gyroscopes, and accurate gyroscopes are generally bulky [11]. For outdoor applications, this type of aiding is very effective, assuming the declination angle is known. For indoor applications, the use of electronic compasses is not as straight forward. As mentioned in Section 2.1, there are many disturbances present in the indoor environment. While there are a number of different ways to reduce the impacts of these disturbances, the heading provided in indoor applications still does not meet the accuracy needs of many indoor applications [8].

Titterton and Weston suggest using a map of magnetic anomalies to estimate the vehicle’s position [11]. This method relies on magnetic anomaly maps and the stability of such anomalies. However, since the anomalies are the measurement, the anomalies will not interfere with the measurements like when using an electronic compass indoors for heading reference [8]. Instead, assuming they are stable over some time period, or vary in a quantifiable way, the more variations in a given location, the more unique the magnetic “fingerprint” [2]. Figure 2 shows an example of this “fingerprint” for an indoor environment.

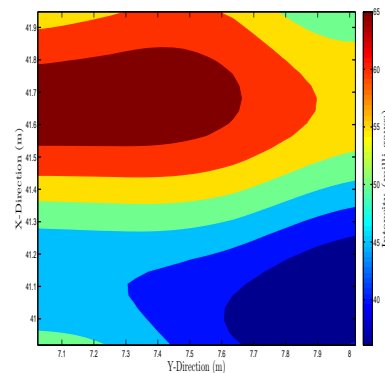


Figure 2: Map of a one square meter magnetic fingerprint generated from magnetic field data collected in a hallway at the Air Force Institute of Technology.

This technique has been demonstrated in the out-

door environment on an aircraft [12]. Wilson, Kline-Schoder, Kenton, Sorenson, and Clavier use maps of “aeromagnetic anomalies”, which are found by taking the difference of the expected magnetic magnitude and the actual measured local field [12]. The approach outlined in [12] uses only the magnitudes of the magnetic field anomaly vectors. By doing this, Wilson et al. do not take advantage of all the information available from the magnetic field.

The experiment presented in this current paper is conducted using a three-axis magnetometer, but the three measured values are then combined to find the total magnitude of the magnetic field. The terrain navigation approach outlined in the next section will show a way to use these three different values together, in order to generate a position solution.

2.3 Magnetic Field Navigation Using a Terrain Navigation Approach

Modern terrain navigation methods often use multiple beams to measure a broader area, which provides more information, hence making it easier to pinpoint the vehicle’s position [7]. The terrain navigation approach described by Nygren in [7] describes a method for combining multiple depth measurements with some sort of navigation system (i.e. INS, Doppler velocity log (DVL), or a system that measures how far the submarine has traveled by counting propeller turns) to determine a submarine’s position.

Nygren’s method begins by defining the system model as

$$\mathbf{x}_{t+1} = \mathbf{x}_t + \mathbf{u}_t + \mathbf{v}_t; \quad t = 0, 1, 2, \dots \quad (1)$$

$$\mathbf{y}_t = \mathbf{h}(\mathbf{x}_t) + \mathbf{e}_t \quad (2)$$

where \mathbf{u}_t is defined as the displacement from the previous position, \mathbf{x}_t , at time t , \mathbf{v}_t is the random error associated with the navigation system that provided \mathbf{x}_t , $\mathbf{h}(\mathbf{x}_t)$ is the function that maps a specific value of \mathbf{x}_t to the measurement domain, and \mathbf{y}_t is the actual measurement collected by the sensor, which has a measurement error, \mathbf{e}_t [7]. Equation 1 is defined as the propagation equation and Equation 2 is the measurement equation [7]. These equations are combined using the standard KF equations.

If \mathbf{e}_t is Gaussian, the likelihood function is

$$L(\mathbf{x}_t; \mathbf{y}_t) = \frac{1}{\Gamma} \exp \left(-\frac{1}{2\sigma_e^2} \sum_{k=1}^N (y_{t,k} - h_k(\mathbf{x}_t))^2 \right) \quad (3)$$

$$\Gamma = \sqrt{\left((2\pi)^N \sigma_e^2 \right)}$$

where σ_e^2 is the measurement error variance and N is the number of measurements to be incorporated [7]. Equation 3 is a mathematical way to determine how well a measurement correlates to the information contained in the map [7]. Therefore, the maximum value of $L(\mathbf{x}_t; \mathbf{y}_t)$ is located at the point most likely to be the position of the vehicle. Nygren points out that if this information is used by itself, then the position estimate is considered a maximum likelihood estimate (MLE). For the case of the submarine, or any vehicle with an additional navigation system, the MLE can be combined with the position estimate from the propagation equation using Bayes’ rule [7]. As defined in [4], Bayes’ rule is

$$P[B|A] = \frac{P[A \cap B]}{P[A]}, \quad (4)$$

which can be written equivalently as

$$P[B|A] = \frac{P[A|B] P[B]}{P[A]}, \quad (5)$$

where $P[A|B]$ is the probability of A given all values of B .

For this application, $P[B|A] = p(\mathbf{x}_{t+1}|\mathbf{Y}_{t+1})$, $P[A|B] = L(\mathbf{y}_{t+1}|\mathbf{x}_{t+1})$, $P[B] = p(\mathbf{x}_{t+1}|\mathbf{Y}_t)$, and $P[A]$ becomes a normalizing constant, C , to ensure the result integrates to one [7]. Notationally, \mathbf{Y}_{t+1} and \mathbf{Y}_t represent all measurements \mathbf{y} up to and including \mathbf{y}_{t+1} and \mathbf{y}_t . The result of this is that the posterior probability density function (pdf), meaning the pdf associated with the position estimate after the position measurement is incorporated, is found by combining the propagated position pdf with the result of Equation 3. Mathematically, this can be written as

$$p(\mathbf{x}_{t+1}|\mathbf{Y}_{t+1}) \sim \frac{L(\mathbf{y}_{t+1}|\mathbf{x}_{t+1}) p(\mathbf{x}_{t+1}|\mathbf{Y}_t)}{C}. \quad (6)$$

Once the posterior pdf is found, the position measurement can be calculated using the point of maximum likelihood, found using Equation 3, as the position measurement and the uncertainty associated with this position measurement, R , is the radius of curvature of the posterior pdf at the point of maximum likelihood [7]. Then, as outlined by Nygren, the position estimate is updated using this measurement data and a KF.

3 Magnetic Field Aided Position Algorithm

Based on the method outlined in Section 2.3, the magnetic field aided position algorithm requires a map of magnetic field intensities for each magnetometer axis and a system model prior to implementation.

3.1 Map of Magnetic Field Intensities

The map of magnetic field intensities can be generated for the entire area where navigation is to occur. This method requires the map to be generated prior to implementation of the positioning algorithm [9]. This method is used to determine a vehicle's location with respect to a specific area.

3.2 Test Environment

The environment chosen to demonstrate the magnetic aided position algorithm was two connected hallways near the Advanced Navigation Technology (ANT) Center at the United States Air Force Institute of Technology (AFIT). Figure 3 is a blueprint of the area used for this experiment, with the actual hallways used outlined in red.

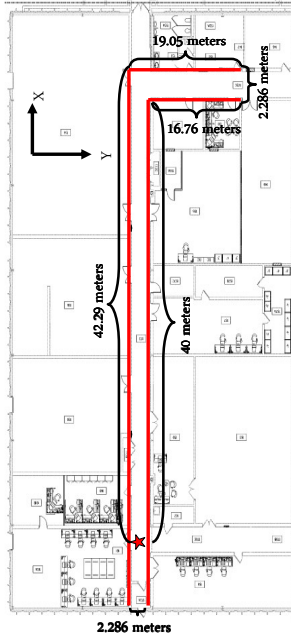


Figure 3: Layout of test environment used for testing the magnetic field aided position algorithm. The area is a hallway at the Air Force Institute of Technology.

A right-handed, Cartesian reference frame is used in the development of the algorithm, with the Z -axis being positive in the downward direction. Figure 3 shows the navigation reference frame in relation to the hallway. The positive X -axis is considered forward from the starting location (which is denoted by a star in Figure 3), while the Y -axis extends from left to right.

The three-axis magnetometer used for this research was the Honeywell HMR2300[®]. The HMR2300[®] is a stand-alone three-axis magnetometer designed to provide magnetic field intensity informa-

tion for a number of applications. Figure 4 shows the HMR2300[®] as used in this research. The HMR2300[®] has a measurement range of ± 2 gauss with a resolution of $< 70 \mu\text{gauss}$ [3]. For reference purposes, the Earth's magnetic field ranges from approximately .3 gauss at the equator to .6 gauss at the poles [10]. Based on the magnitude of the Earth's magnetic field intensity, the selected magnetometers should be able to measure all variations about the Earth's main field.



Figure 4: Photo of the Honeywell HMR 2300 as packaged for research

3.3 System Model

The dynamics model used to test the magnetic field aided position algorithm is defined in the navigation frame as

$$\begin{bmatrix} \dot{P}_Y \\ \dot{P}_X \\ \dot{V}_Y \\ \dot{V}_X \end{bmatrix} = \underbrace{\begin{bmatrix} 0 & 0 & 1 & 0 \\ 0 & 0 & 0 & 1 \\ 0 & 0 & 0 & 0 \\ 0 & 0 & 0 & 0 \end{bmatrix}}_{\mathbf{F}(t)} \underbrace{\begin{bmatrix} P_Y \\ P_X \\ V_Y \\ V_X \end{bmatrix}}_{\mathbf{x}(t)} + \underbrace{\begin{bmatrix} 0 & 0 \\ 0 & 0 \\ 1 & 0 \\ 0 & 1 \end{bmatrix}}_{\mathbf{B}(t)} \underbrace{\begin{bmatrix} u_{V_Y} \\ u_{V_X} \end{bmatrix}}_{\mathbf{u}(t)} \quad (7)$$

$$+ \underbrace{\begin{bmatrix} 0 & 0 \\ 0 & 0 \\ 1 & 0 \\ 0 & 1 \end{bmatrix}}_{\mathbf{G}(t)} \underbrace{\begin{bmatrix} w_{v_Y} \\ w_{v_X} \end{bmatrix}}_{\mathbf{w}(t)}$$

where P_Y and P_X are the positions in the X and Y directions, u_{V_Y} and u_{V_X} are the control inputs used to control the velocity, and w_{v_Y} and w_{v_X} are the white, Gaussian noises driving the system, which are characterized by $E[\mathbf{w}(t)\mathbf{w}^T(t + \tau)] = \underbrace{\begin{bmatrix} \sigma_v^2 & 0 \\ 0 & \sigma_v^2 \end{bmatrix}}_{\mathbf{Q}} \delta(\tau)$. The

relationship between the body frame and the navigation frame is defined as

$$\begin{bmatrix} V_Y \\ V_X \end{bmatrix} = \begin{bmatrix} \cos(\psi) & \sin(\psi) \\ -\sin(\psi) & \cos(\psi) \end{bmatrix} \begin{bmatrix} V_{bY} \\ V_{bX} \end{bmatrix}. \quad (8)$$

For the purposes of this research, the heading angle, ψ , is assumed to be known at all times.

4 Position Algorithm Implementation

In terrain navigation, certain features or characteristics must be matched to determine the position and then that matched position is used as the position measurement for the KF. The same holds true when using magnetic field intensity data [12, 2]. The magnetometers measure the magnetic field intensity and then the measurement generation algorithm determines how this measurement relates to the vehicle's position via a mapping function [7].

Using the process outlined in Section 2.3, the first step in finding the position associated with a particular measurement is to combine the propagated pdf with the result of the likelihood function to determine the location that best matches the magnetic reading. This is accomplished by:

1. Calculating the likelihood function for all possible locations.
2. Generating a discrete pdf that accurately describes the propagated position estimate.
3. Combining the results from steps 1 and 2 using Equation 6 to determine the position measurement, which is located at the maximum of the resulting pdf.
4. Calculating the measurement noise intensity, R .

4.1 Example Likelihood Function Result

The first step in the magnetic aided position algorithm is calculating the result of Equation 3, with $N = 3$. The measurements for this example were simulated based off of the truth data used in generating the map. For this example, it is clear that there are three peaks. Any one of these peaks could be the actual location of the vehicle. This result is combined with the bivariate Gaussian pdf using Bayes' rule, as discussed in Section 2.3.

4.2 Example Discrete Bivariate Gaussian PDF

With the likelihood function calculated, the next step in the position algorithm is to generate the discrete bivariate, Gaussian pdf that describes the discrete KF estimate. This pdf is centered around the propagated state estimate and uses the associated propagated filter uncertainties. For the example pictured in Figure 6, the position state estimate is $\hat{\mathbf{x}}(t_k^-) = \begin{bmatrix} 1.1565 \\ 2.2438 \end{bmatrix}$ and

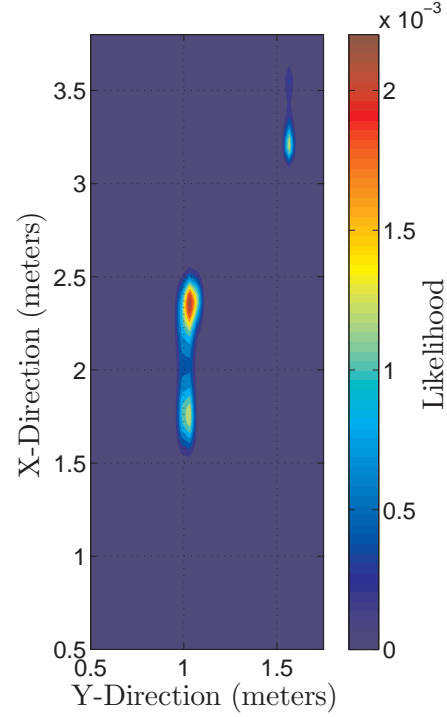


Figure 5: Example discrete likelihood function result that will be combined with the result of the discrete probability density function using Bayes' rule

$$\mathbf{P}(t_k^-) = \begin{bmatrix} 0.0513 & 0 \\ 0 & 0.4837 \end{bmatrix}.$$

4.3 Bayes' Rule Implementation Example

The result of combining the likelihood function and the bivariate Gaussian pdf is shown in Figure 7. Since the two peaks of the likelihood function were so closely positioned, both are still present after combination with the pdf. However, the magnitudes of these peaks have been scaled according to their location from the filter's estimated position. The difference between the height of the peak located at approximately (1.75,1) and the one located at approximately (2.4,1) is now noticeably larger. Also notice that the peak located at approximately (1.5,3.2) is completely removed.

Choosing the point of maximum likelihood from the combination of the propagated pdf and the likelihood result could result in the wrong location being chosen. Choosing the wrong location could prevent the magnetic aided position algorithm from accurately estimating its position. In order to reduce the effects of bad measurements, several options could be implemented following the combination of the pdf and the likelihood function. One method would be residual monitoring. If a measurement is so many meters away from the estimate (this value would be determined based on your system model), that measure-

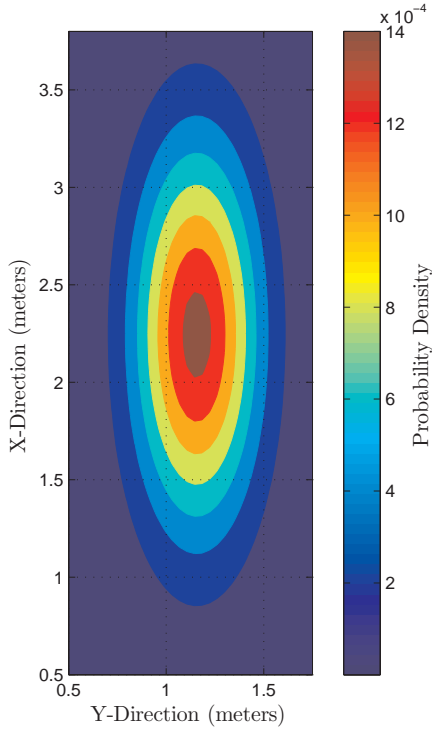


Figure 6: Example discrete propagated probability density function that will be combined with the result of the likelihood function using Bayes' rule.

ment would be ignored. Another method would be to ignore a measurement if there were multiple peaks within a pre-determined area, this area would be determined by the uncertainty of the system model.

4.4 Measurement Noise Intensity

It is known that the KF needs a value for the measurement noise intensity to operate properly. For applications such as GPS, the measurement noise of the GPS measurement is the value assigned to R . In this case, that will not be sufficient because the measurements generated by the magnetometers are transformed into position measurements, but the errors are not directly transformed from a unit of magnetic field intensity to a unit of length. In addition to the errors not being in the proper units, any information that could be gained from the post-Bayes' rule pdf is dependant upon the filter's uncertainty and, for a KF, the process noise and the measurement noise (i.e., $\mathbf{Q}(t_k)$ and $\mathbf{R}(t_k)$, respectively) need to be uncorrelated or accounted for by an augmented state matrix. The method proposed by Nygren in [7] uses the radius of curvature of the posterior pdf to calculate R , but then augments the KF to account for this correlated noise. Instead of using the correlated noise method, a new method was developed to remove the correlation.

The new process begins with the point of maxi-

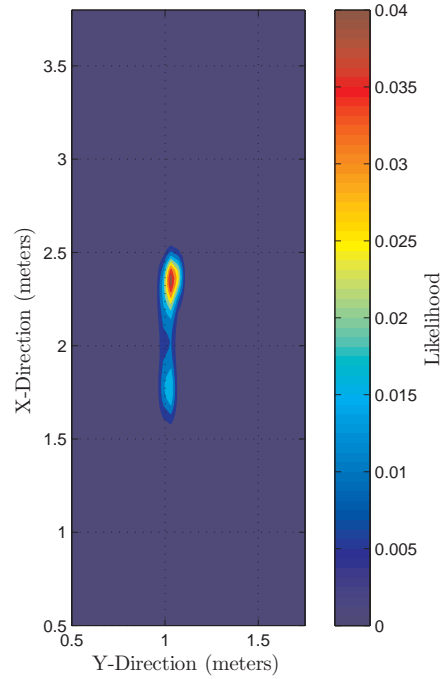


Figure 7: Example discrete post-measurement probability density function generated using Bayes' rule to combine Fig. 6 with Fig. 5.

imum likelihood. Using this point as the center, an array of indices is created in the X -direction and in the Y -direction. The measured magnetic field intensity is then compared with the magnetic field intensities of the surrounding locations using Equation 3. The result of the likelihood function is then normalized to make the result a pdf. The standard deviations of the two resulting pdfs (one for the X -direction and one for the Y -direction) will be the square root of the measurement noise intensity, or the standard deviation of the dataset. For a Gaussian pdf, $\sim 68\%$ of the data is included within a 1σ -band. To calculate the standard deviation of experimental pdfs, the point on the left side of the mean where $\sim 16\%$ of the data is in the tail can be found and the same for the right tail. The distance that these two points are from the mean of the pdf are then averaged to calculate the standard deviation (σ_Y and σ_X) of the measurement noise intensity, resulting in $\mathbf{R} = \begin{bmatrix} \sigma_Y^2 & 0 \\ 0 & \sigma_X^2 \end{bmatrix}$.

5 Results

The first test conducted to demonstrate the trajectory estimation capability of this algorithm used a 100 Monte Carlo (MC) run simulation, which was based on the real hallway magnetic field intensity map. Each MC run consisted of a randomly generated trajectory using the system model described in Equation 7 and the parameters shown in Table 1. The trajectory gen-

Table 1: Parameter values used for the simulations that demonstrate the magnetically aided navigation system.

Parameter	Value
Time Step Δt	0.1 sec
Initial X -Direction Velocity (V_X)	.5 m/s
Initial Y -Direction Velocity (V_Y)	0 m/s
Initial Filter X -Position (P_X)	0 m
Initial Filter Y -Position (P_Y)	0 m
Initial Vehicle X -Position (P_X)	0 m
Initial Vehicle Y -Position (P_Y)	1.145 m
Initial X -Pos. Uncertainty (σ_{P_X})	1.5 m
Initial Y -Pos. Uncertainty (σ_{P_Y})	1.5 m
Velocity Uncertainty Both Axes (σ_v)	.08 m/ \sqrt{s}
Magnetometer Meas. Noise (σ_{meas})	1 milli – gauss
Filter Update Interval	1.5 sec

eration process showed that $\sigma_v = .08 \text{ m}/\sqrt{s}$ was too large to keep the vehicle within the bounds of the hallway without some sort of control action. Therefore, for the purposes of the simulation, a controller was implemented to ensure that the generated cross-track position (P_Y for the main hallway and P_X for the side hallway) was within the physical bounds of the hallway.

Figure 8 shows that the magnetic aided position algorithm is accurate to within .2 meters when estimating a random trajectory. The covariance analysis can be seen in Figure 9. The effect of the controller used to keep the random trajectory within the physical bounds of the hallway can be seen in Figure 9. The effect is that the filter has a more pessimistic estimate of its uncertainty in the Y -direction prior to the travel direction change and, following the turn, a more pessimistic estimate of the uncertainty in the X -direction.

The second test conducted used real measurements along a specific trajectory. Figure 10 shows the trajectory used for the real measurement test. The process noise added to the system was reduced to reflect the lack of variation in the true trajectory. The result of using the real measurements are shown in Figure 11. The errors are less than .2 meters for the majority of the trajectory.

6 Conclusions

This research has demonstrated the feasibility of using magnetic field intensities to aid in indoor navigation. When using a map of the entire test environment, the

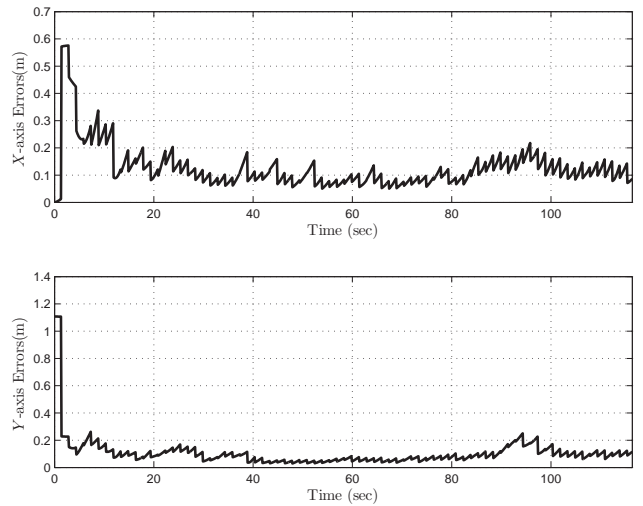


Figure 8: The RMS values for 100 MC runs using the magnetic aided position algorithm.

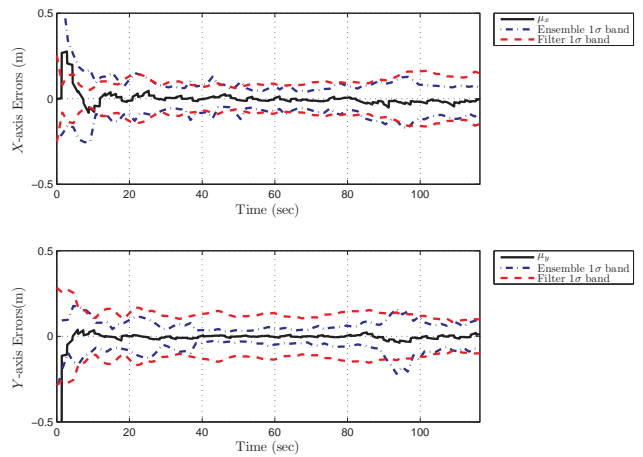


Figure 9: The filter's ability to track the trajectory is contingent on the filter having the correct system model. In this case, the system model is correct and the filter and ensemble statistics match fairly well, which shows the system model is accurate.

magnetic aided position algorithm is able to accurately estimate its position to within .3 meters.

While this research investigates the feasibility of using magnetic field intensities to aid navigation, it does not directly investigate the stability of the indoor magnetic fields with respect to time. The real measurements were collected two weeks after the map data they were compared with. This shows that there is some stability with respect to time, but further research should investigate the limits of this stability.

Another area for future research is in the area of determining the best sensor alignment on the vehicle to maximize performance. Performance of the vehicle tracking algorithm could be greatly increased if multiple magnetometers were used on the vehicle. By

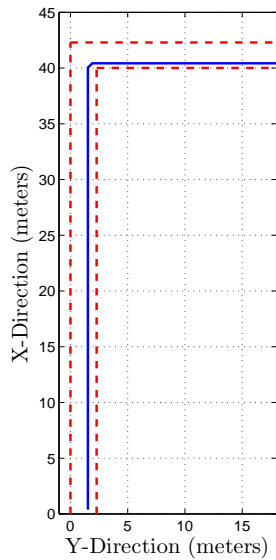


Figure 10: Real trajectory near right side of hallway. This trajectory was used to demonstrate the performance of the magnetic aided position algorithm using real measurements.

adding additional sensors, the vehicle would be able to use the geometry of its sensor array to help determine which peaks from the post-Bayes' rule combination are valid.

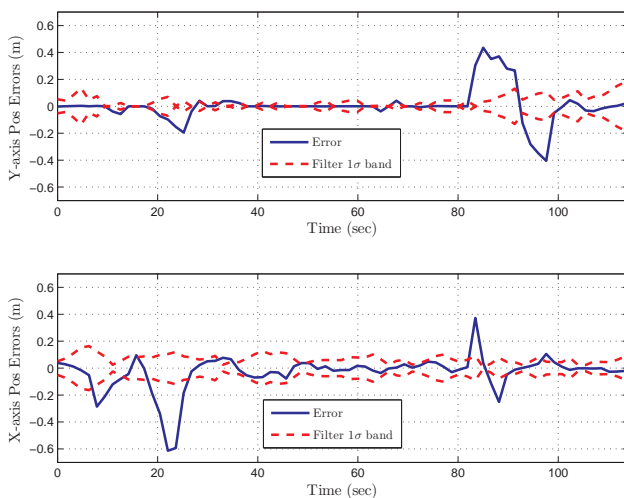


Figure 11: Position error plots showing the filter performance using the real measurements from the trajectory shown in Figure 10.

References

- [1] Campbell, Wallace Hall. *Earth Magnetism: A Guided Tour through Magnetic Fields*. Complementary Science Series. Harcourt/Academic Press, San Diego, CA, 2001.
- [2] Goldenberg, Felix. "Geomagnetic navigation beyond the magnetic compass". *Record - IEEE PLANS, Position Location and Navigation Symposium, IEEE/ION Position, Location, and Navigation Symposium*, 2006:684–694, 2006.
- [3] Honeywell, Solid State Electronics Center. "HMR2300 Smart Digital Magnetometer Datasheet". <http://www.ssec.honeywell.com/magnetic/datasheets/hmr2300.pdf>.
- [4] Leon-Garcia, Alberto. *Probability and random processes for electrical engineers*. Addison-Wesley Publishing Company, Inc., Reading, MA, 2 edition, May 1994.
- [5] Misra, Pratap and Per Enge. *Global Positioning System: Signals, Measurements, and Performance*. Ganga-Jamuna Press, Lincoln, MA, second edition, 2006.
- [6] Nelson, James H., Loius Hurwitz, and David G. Knapp. *Magnetism of the Earth*. Publication 40-1, United States Department of Commerce: Coast and Geodetic Survey, Washington D.C., 1962.
- [7] Nygren, Ingemar. "Robust and efficient terrain navigation of underwater vehicles". *Position, Location and Navigation Symposium*, 923–932. IEEE/ION, 2008.
- [8] Skvortzov, Vladimir Y., Hyoung-Ki Lee, Seok-Won Bang, and YongBeom Lee. "Application of Electronic Compass for Mobile Robot in an Indoor Environment". *International Conference on Robotics and Automation*, 2963–2970. Institute of Electrical and Electronics Engineers, Rome, Italy, April 2007.
- [9] Storms, William F. and John F. Raquet. *Magnetic Field Aided Indoor Navigation*. Master's thesis, Air Force Institute of Technology, March 2009.
- [10] Strangway, David W. *History of the Earth's Magnetic Field*. McGraw-Hill, Inc., New York, NY, 1970.
- [11] Titterton, David H. and John L. Weston. *Strap-down Inertial Navigation Technology*. The Institution of Electrical Engineers, Michael Fara-

day House, Six Hills Way, Stevenage, Herts. SG1 2AY, United Kingdom, 2004.

- [12] Wilson, John M., Robert J. Kline-Schoder, Marc A. Kenton, Paul H. Sorensen, and Odile H. Clavier. “Passive Navigation Using Local Magnetic Field Variations”. *Institute of Navigation International Technical Meeting*, 770–779. Institute of Navigation, Monterey, CA, January 2006.